International Journal of Environmental Sciences
ISSN: 2229-7359
Vol. 10 No. 4, 2024
https://theaspd.com/index.phpa

Evaluation of the Anti-Obesity Potential of Ginseng Flower Bud Extract

Linjun Liu[1], Sreemoy Kanti Das[2*]
[1,2]Faculty of Pharmacy, Lincoln University College, Petaling Jaya, Malaysia
[1]liulinjun.masterscholar@lincoln.edu.my
0009-0001-5397-8841
Email of corresponding author: sreemoy@lincoln.edu.my

ABSTRACT
Background: Ginseng flower buds, a part of the ginseng plant, are known to be rich in ginsenosides, which are the active compounds attributed to ginseng's pharmacological effects. Although substantial scientific data have been accumulated regarding the pharmacological activities of ginseng roots, the therapeutic potential of ginseng flower buds has been largely overlooked. In this study, HepG2 cells treated with a free fatty acid mixture and hepatocytes isolated from rats fed a high-fat diet for three weeks were utilised as in vitro models of hepatic steatosis to evaluate the anti-steatotic effects of the extract[1]. Methods: The effects of ginseng flower buds were further investigated under pathologic conditions of hepatic steatosis induced by a high-fat diet over 12 weeks in C57BL/6J mice. A comprehensive analysis of hepatic gene expression profiles was conducted in mice treated with ginseng flower bud extract. Quantitative PCR was performed to validate the impact of the ginseng flower bud extract on the expression profiles of selected genes. Results: Treatment with ginseng flower bud extract significantly reduced the lipid droplets stained by Oil Red O and intracellular triglyceride levels in HepG2 cells and rat hepatocytes. In high-fat diet-fed mice, ginseng flower bud therapy (500 mg/kg) resulted in a marked reduction in histological signs of hepatic steatosis, with hepatic triglyceride levels reduced by 34.1% compared to the high-fat diet group[2]. These effects were accompanied by further improvements in insulin signalling. Global gene expression analysis revealed that ginseng flower bud treatment could reverse the hepatic gene expression profile associated with steatotic livers, with regulated genes involved in immune processes, insulin response, and lipid storage. Conclusion: The study provides strong evidence that ginseng flower buds may prevent or treat non-alcoholic fatty liver disease (NAFLD) by inhibiting hepatic inflammation and fatty acid uptake, and by enhancing hepatic insulin signalling pathways.
Keywords: *Ginseng flower buds; Ginsenosides; Animal models; Data analysis*

INTRODUCTION

Ginseng flower bud extract possesses significant therapeutic potential, demonstrating notable effects in the prevention and treatment of various diseases, which suggests it may serve as a novel health supplement. Current research indicates that ginseng flower bud extract can enhance immune system function, reduce inflammation, improve cardiovascular health, exhibit anti-ageing properties, alleviate pain, combat cancer, and potentially aid in the treatment of neurological disorders[3].

The primary chemical constituents of ginseng flower buds include ginsenosides, flavonoids, volatile oils, and polysaccharides. The major active components are ginsenosides, predominantly presented as white amorphous powders or colourless crystals, classified as steroidal saponins belonging to the triterpene saponins. The ginsenoside content in ginseng flower buds is several times higher than that found in ginseng roots, and they are particularly rich in ginsenoside Rd, which inhibits cancer cell growth and enhances immune function. Additionally, they contain vitamins, amino acids, and other beneficial compounds.

Ginsenosides from ginseng flower buds have been shown to enhance both innate and adaptive immune responses, promote the production of specific antibodies, and exhibit anti-tumour and anti-ageing effects. Historical references to ginseng, such as in the "Shennong Ben Cao Jing," describe its long-term use for promoting longevity and vitality. Ginsenosides in ginseng flower buds may inhibit cerebral ischemia and increase superoxide dismutase (SOD) activity in brain tissue by upregulating SOD gene expression, similar to the pharmacological effects observed with ginseng root saponins[4].

Non-medicinal parts of ginseng and American ginseng have demonstrated substantial anti-tumour activity, including the ability to alleviate tumour-related complications and mitigate the side effects of chemotherapeutic agents when used in combination. The polysaccharides in ginseng flower bud extract, due to their immunomodulatory effects, hold promise as potential agents for the active treatment and prevention of tumours. The addition of ginseng flower bud extract to the Fenton reaction system (GSE142059) has been shown to effectively scavenge hydroxyl radicals (·OH), with optimal efficacy

observed at a ginsenoside concentration of 12.30 μg/μl. Moreover, ginseng flower bud extract has been demonstrated to significantly improve hypercoagulability and anaemia in cancer model mice, suggesting its potential as a therapeutic agent in cancer treatment. Pre-treatment with components from ginseng flower bud extract can also alleviate chemotherapy-induced nausea and vomiting and restore food intake in rats.

Ginseng flowers can be processed into tea, which has been found to relieve fatigue, enhance immunity, and promote overall health. The total ginsenoside content in ginseng flowers is considerably higher than in ginseng roots. Developing health beverages from ginseng flowers utilises this valuable by-product of ginseng cultivation, offering anti-fatigue effects and regulating the body's cAMP-cGMP balance.

MATERIALS

GSE142059 is an expression matrix dataset related to the effects of ginseng flower bud extract in preventing hepatic steatosis by improving liver inflammation and insulin resistance. The dataset was downloaded using the getGEO() function from the GEOquery package (version 2.66.0) in R. The dataset includes nine samples divided into three groups, each with three replicates: the RD group (regular diet), the HFD group (high-fat diet), and the GFB group (high-fat diet + ginseng flower bud extract). In the getGEO() function, the first argument is the GEO dataset accession number, "GSE142059" in this case. The second argument, GSEMatrix, is set to TRUE to obtain the data matrix, and the third argument, AnnotGPL, is set to TRUE to retrieve annotation information.

METHOD

A boxplot was used to visualise the expression levels of the samples.

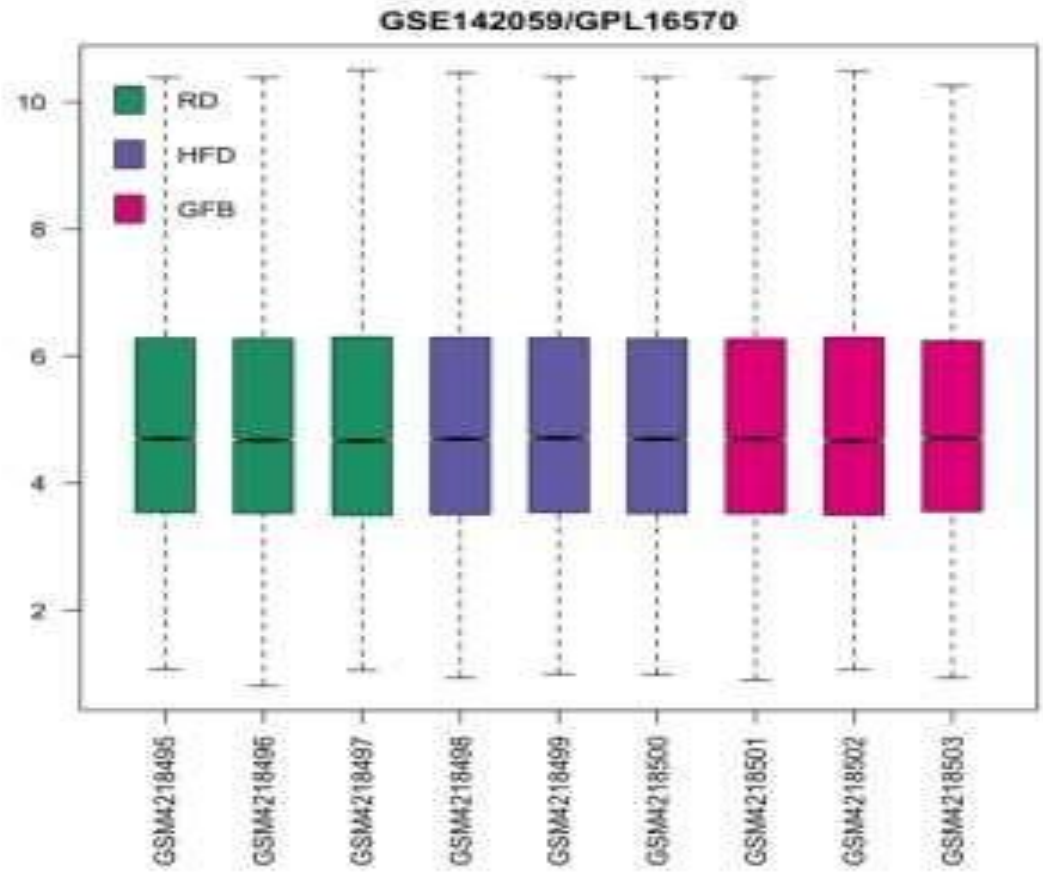

Figure1: Boxpl

As shown in Figure 1, the overall expression levels across all samples are on a similar horizontal line, indicating comparability among the samples. To further examine group differences, UMAP (Uniform Manifold Approximation and Projection) was employed for dimensionality reduction.

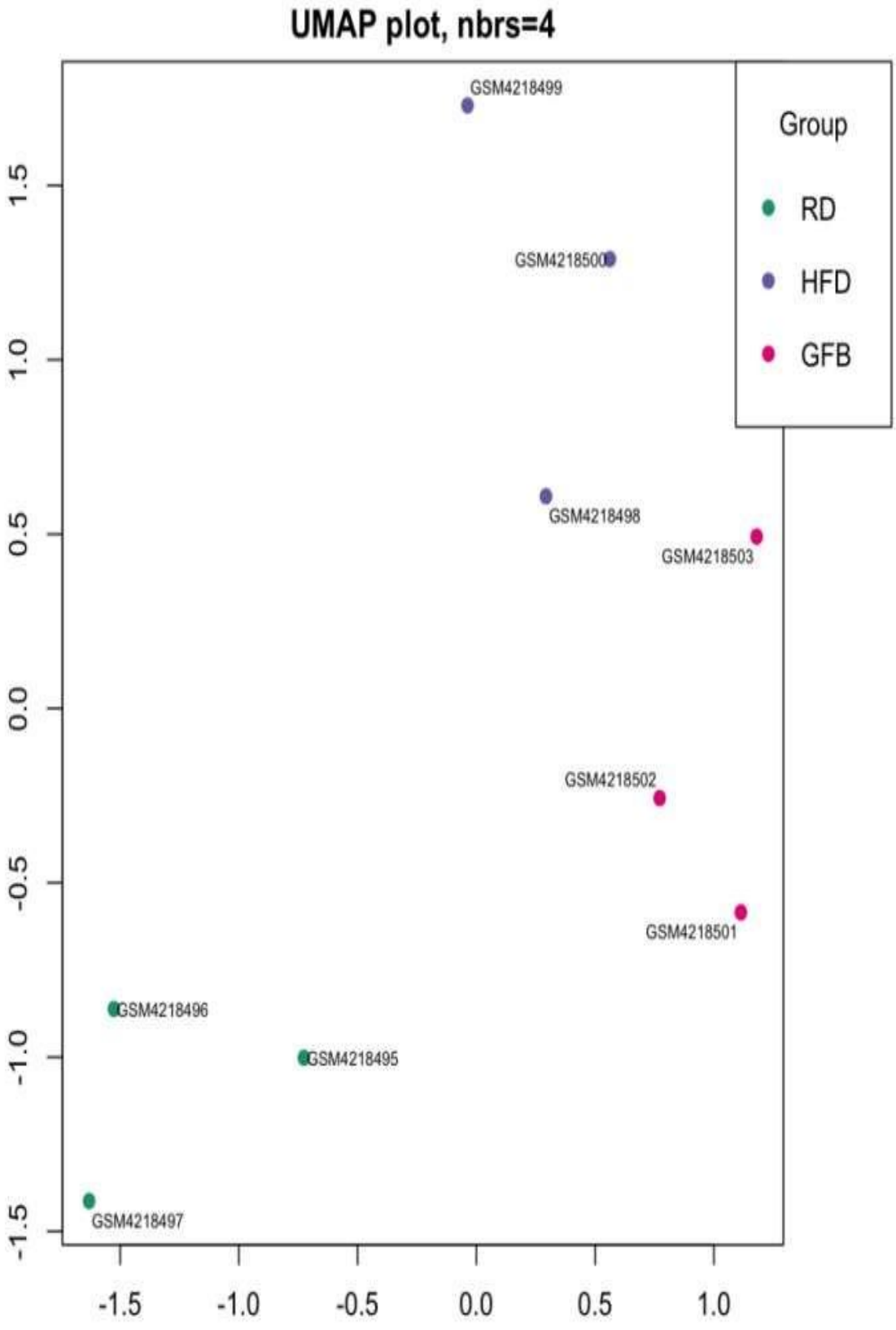

Figure2: Umap

As shown in Figure 2, the UMAP plot illustrates that the three samples within the same group are clustered closely together, while samples from different groups are further apart. This indicates that the transcriptomic differences within the same group are minimal, whereas the differences between groups are more pronounced.

The script uses if conditions to differentiate between sample groups. If the dataset contains multiple matrices, the index of the matrix containing the desired GPL ID is returned; otherwise, it returns 1. The function pData() retrieves sample information from the dataset, while fvarLabels() returns feature labels. The samples were divided into three groups: RD (regular diet), HFD (high-fat diet), and GFB (high-fat diet + GFB), with the RD group serving as the control. The exprs() function was employed to obtain the expression matrix from the GEO dataset, followed by log2 transformation of the expression matrix.

RESULTS AND DISCUSSION

The GSE142059 dataset comprises 9 samples and 41,345 transcript cluster IDs. After converting these IDs to gene symbols using the Affymetrix Mouse Gene 2.0 ST Array Platform GPL16570, the dataset contained 24,647 gene symbols. Differential gene expression analysis was performed using the limma package, categorising the 9 samples into 3 groups: RD, HFD, and GFB.

Initially, data preprocessing involved converting gene expression levels in the matrix into factors (gs) and labelling each group as "RD," "HFD," or "GFB." A linear model was then fitted using the lmFit() function[5]. The makeContrasts() function was employed to generate required contrasts, followed by the contrasts.fit() function to recalculate model coefficients. Statistical analysis was conducted using the eBayes() function for Bayesian adjustment, yielding adjusted significance levels. The topTable() function was used to extract the top 500 most significantly differentially expressed genes, categorised by direction of expression (upregulated, downregulated, or unchanged) using the decideTests() function. The top 10 most significant genes, ranked by F-value and p-value, were C730002L08Rik, Sqle, Slc23a1, Enpp2, Idi1, Tmem184c, Steap4, Saa4, Gm10680, and Acot1.

In RNA-seq data analysis, the Q-Q plot (Quantile-Quantile plot) is a graphical method used to evaluate whether the actual data distribution matches the expected distribution. The t-QQ plot compares theoretical quantiles of t-values on the x-axis against the actual quantiles of t-values on the y-axis. If the actual quantiles align perfectly with the theoretical quantiles, the points would lie on a 45-degree diagonal line. Deviations from this line suggest discrepancies between the actual and expected distributions.

A Q-Q plot was generated using "moderated t-values," calculated based on each gene's expression and variability. Specifically, the lmFit() function was used to fit a linear model, and eBayes() was applied to compute the moderated t-values. Missing values (NA) were filtered out using the which() function, and the Q-Q plot was created with qqt(), further screening t-values within t.good. Points deviating from the 45-degree diagonal in the Q-Q plot may indicate data not conforming to the expected distribution.

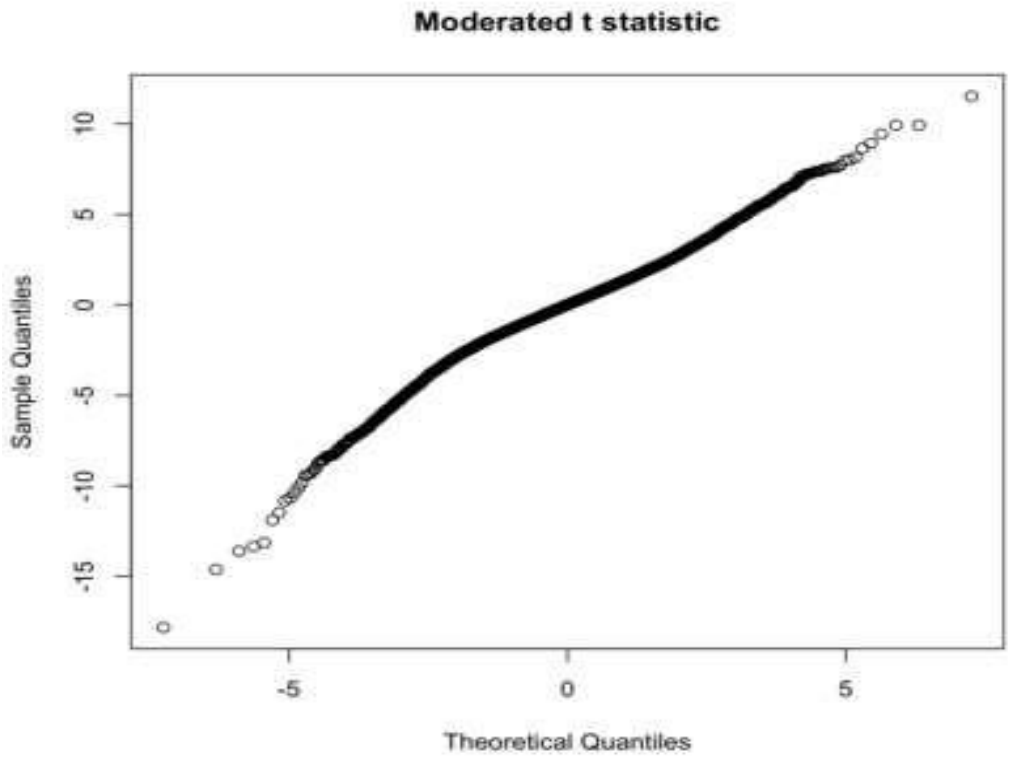

Figure3: The Q-Q diagram of RNA-seq

As shown in Figure 3, there are few points deviating from the 45-degree line in the Q-Q plot, indicating good quality of the RNA-seq data.

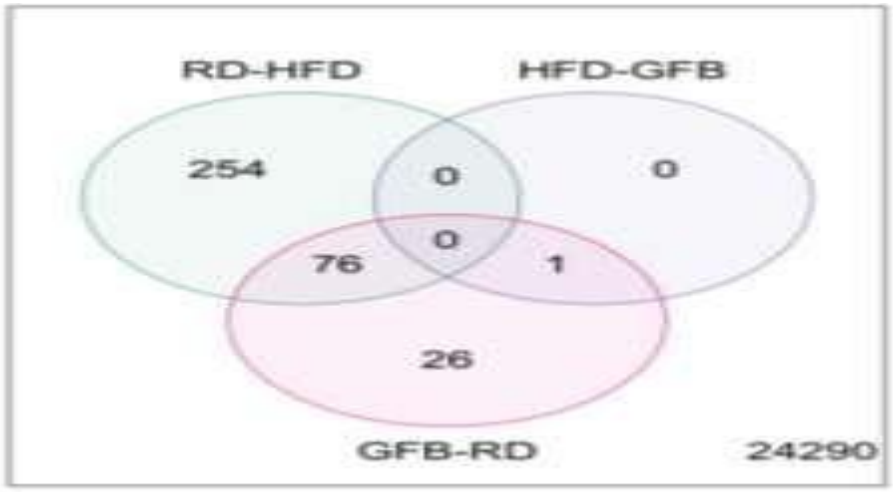

Figure4: Vene plot of the genes in each sample

As shown in Figure 4, the density plot illustrates the gene expression values for each sample. The x-axis represents gene expression values, while the y-axis denotes the density of these expression values. Each sample's density curve is represented in a different colour, allowing for a clear visual comparison of gene expression value distributions across the samples. The plot reveals that the distribution of gene expression values is relatively similar among the different samples.

Using the vennDiagram() function, a Venn diagram of the differential expression results was generated.

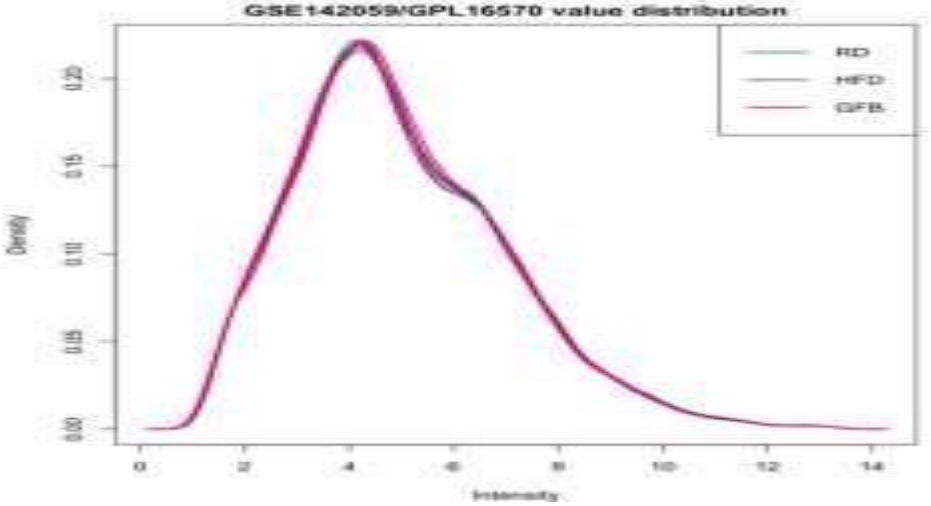

Figure5: The expression densities in each group

As shown in Figure 5, a total of 24,647 genes were analysed, of which 24,290 showed no differential expression. When comparing the RD (regular diet) group and the HFD (high-fat diet) group, 330 differentially expressed genes were identified. In the comparison between the HFD group and the GFB (high-fat diet + GFB) group, only one differentially expressed gene was identified. Comparing the GFB group to the RD group, 103 differentially expressed genes were found, with 76 common differentially expressed genes between the RD-HFD group and the GFB-RD group. There was only one common differentially expressed gene between the GFB-RD group and the HFD-GFB group, and no common differentially expressed genes between the HFD-GFB and RD-HFD groups. A density plot of expression values was also created to visualise the distribution of gene expression values in RNA-seq data.

Volcano and MD plots were generated for each of the three contrast groups to visualise differential gene expression. Figures 6 and 7 illustrate the gene expression comparison between the RD (Regular Diet) and HFD (High Fat Diet) groups[6].

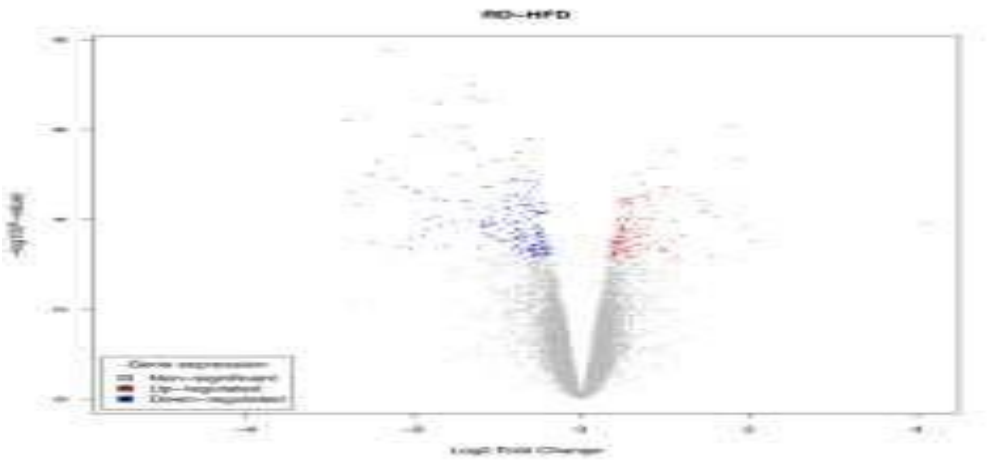

Figure6: Volcano map of the RD-HFD Formation

As shown in Figure 6, the volcano plot was constructed with log10 (P-value) on the y-axis and log2 (fold change) on the x-axis, providing a clear depiction of the significance and magnitude of gene expression changes. Significance is represented by colour coding: blue points indicate significantly downregulated genes, red points indicate significantly upregulated genes, and grey points represent genes without differential expression. The magnitude of expression change is represented by the position of the points on the plot. Notably, the majority of genes are grey, indicating a lack of significant differential expression, while fewer genes show significant upregulation or downregulation.

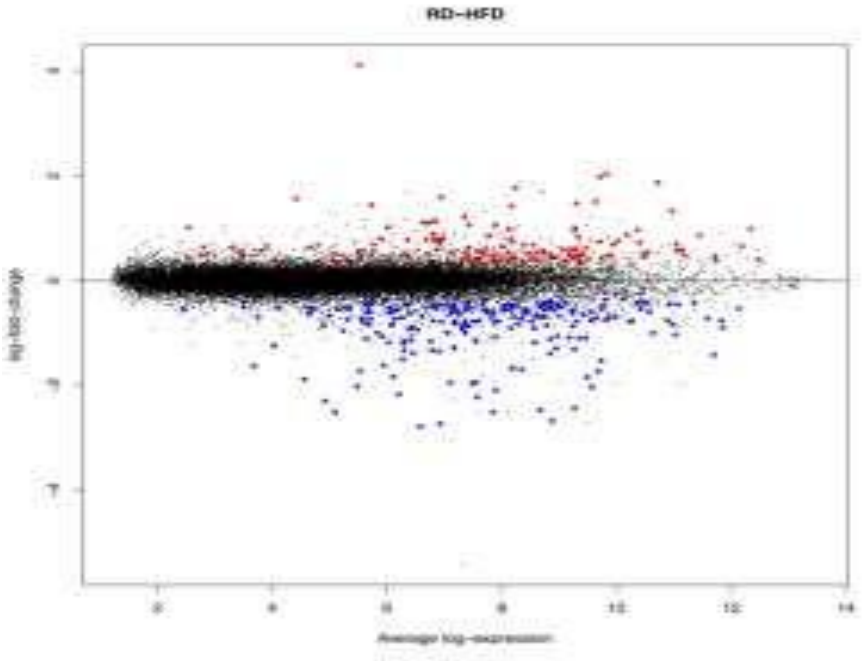

Figure7: MD diagram of the RD-HFD group

As depicted in Figure 7, the MD plot is constructed using log2(fold change) as the x-axis and average expression levels as the y-axis, facilitating the visualisation of the direction and magnitude of gene expression alterations. Similar to a volcano plot, downregulated genes are represented in blue, upregulated genes in red, and genes with no significant difference are depicted in grey.

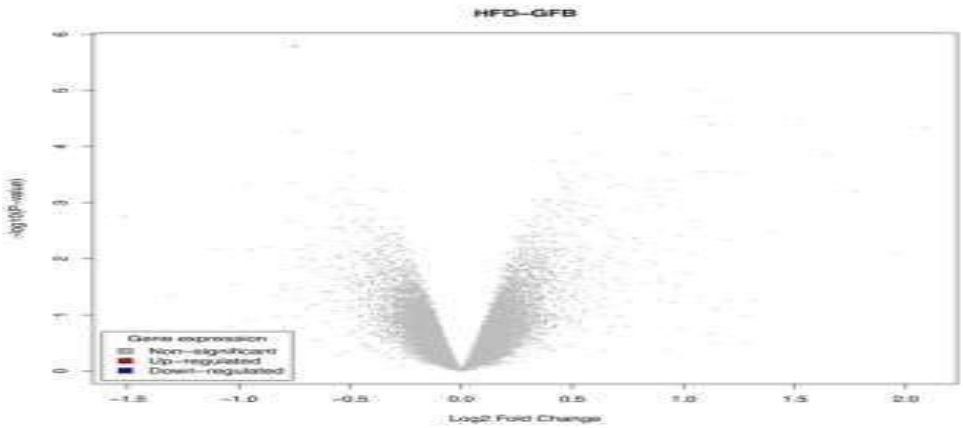

Figure8: Volcano map of the HFD-GFB group

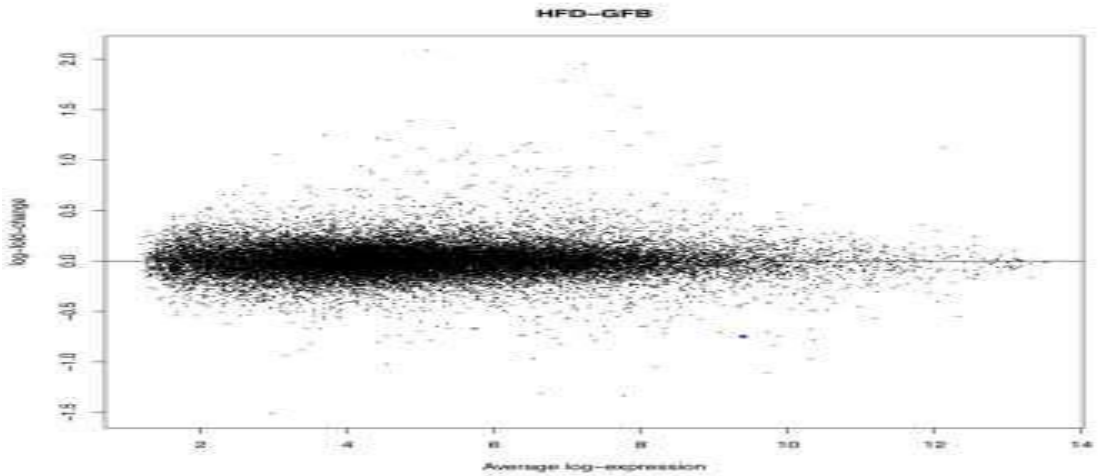

Figure9: MD diagram of the HFD-GFB group

The gene expression patterns in the HFD group relative to the GFB group, as depicted in Figures 8 and 9, indicate that there is a singular gene that exhibits significant downregulation, whereas the vast majority of genes do not display any statistically significant alterations in their expression levels, as discerned from the associated volcano and MD plots.

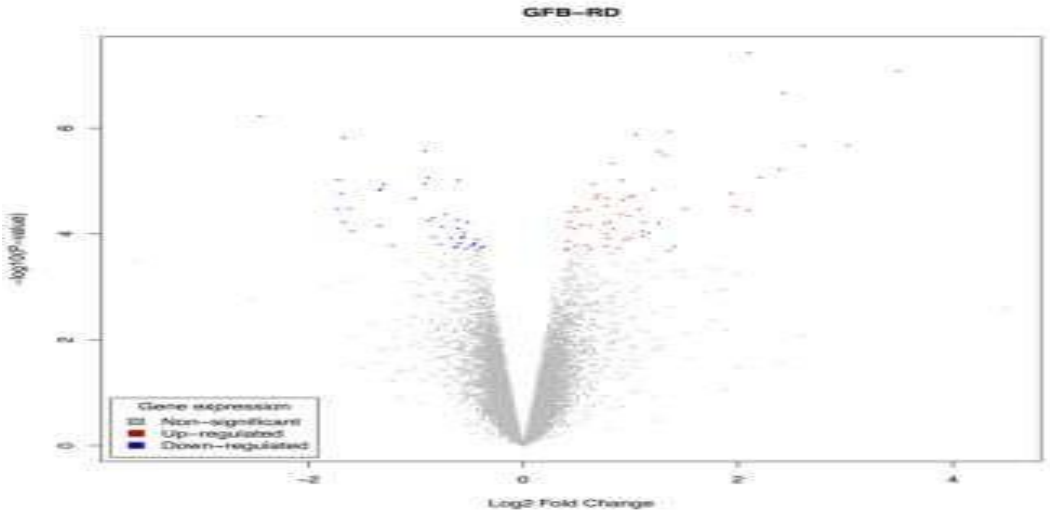

Figure10: Volcano map of the GFB-RD Formation

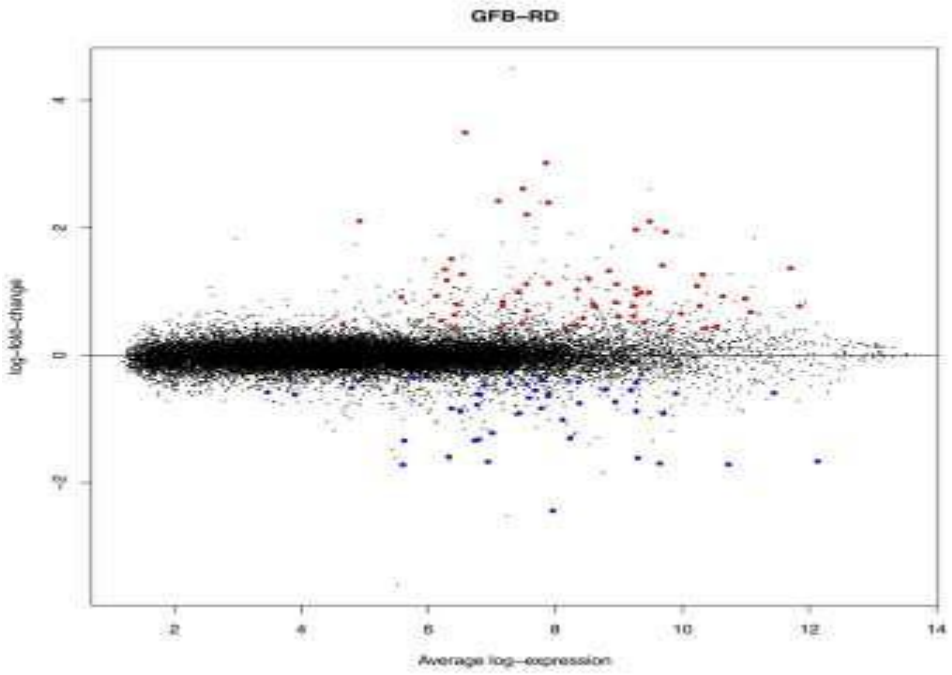

Figure11: GFB-RD group of the MD diagram

As depicted in Figures 10 and 11, an analysis of the gene expression profiles between the GFB group and the RD group via the corresponding volcano and MD plots reveals that the majority of genes exhibit no significant differences in expression. The number of genes with statistically significant upregulation or downregulation is relatively small within this group.

Produce a heatmap of differentially expressed genes to display the changes in expression levels of differentially expressed genes in the RNA-seq dataset.

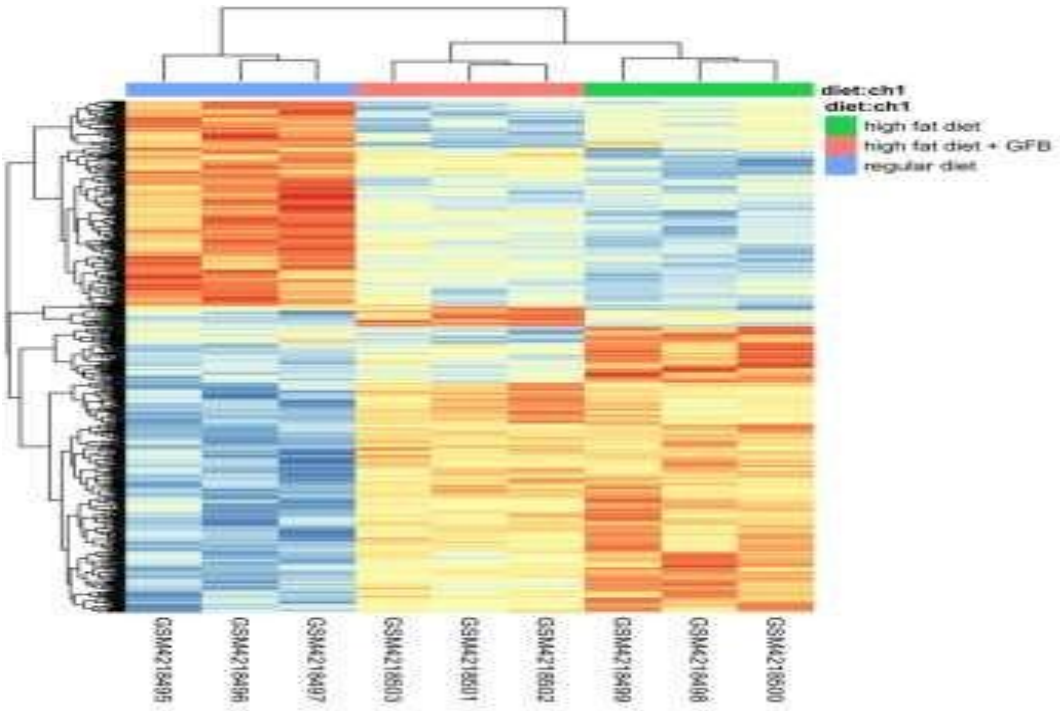

Figure12: Differential gene expression heatmap

Figure 12 shows, the heatmap is composed of two parts, samples and genes. Each sample is represented as a column, and each gene as a row. The color of each cell represents the relative level of gene expression in the sample. A color gradient is used to indicate the expression values, with low expression levels in blue and high expression levels in red. This heatmap facilitates a direct comparative analysis of gene

expression levels across different samples. The heatmap also includes clustering analysis, which groups similar genes or samples together, making it easier to observe changes in the overall expression patterns. In gene clustering, adjacent rows represent similar genes; in sample clustering, adjacent columns represent similar samples. The clustering results provide useful information about gene expression patterns and sample similarity, aiding in the identification of biological characteristics specific to certain genomes and samples

The heatmap reveals that the expression patterns of differentially expressed genes are quite similar within the same group, and the gene expression profiles between the GFB group and the HFD group are very similar[7]. This is consistent with the results from the previous volcano plot, which indicated only one downregulated differentially expressed gene between the GFB group and the HFD group.

For the identified differentially expressed genes, a Gene Ontology (GO) enrichment analysis was conducted. GO is a standardised biological nomenclature system used to describe the functions of genes and proteins. The GO classification is structured into three domains: molecular function, cellular component, and biological process. Through GO annotation, the functions of genes or proteins can be categorised.

Table1: GO-enriched pathway

Categor		Pathway	pvalue	Count	log10 y
GO:0008202	BP	steroid metabolic process	8.53E-19	35	18.06919449
GO:0006520	BP	cellular amino acid metabolic process	3.79E-18	30	17.42102573
GO:0006694	BP	steroid biosynthetic process	6.20E-18	25	17.20742738
GO:0016126	BP	sterol biosynthetic process	3.06E-17	17	16.51370168
GO:0044282	BP	small molecule catabolic process	3.63E-17	33	16.44014524
GO:0006695	BP	cholesterol biosynthetic process	1.32E-16	16	15.88059098
GO:1902653	BP	secondary alcohol biosynthetic process	1.32E-16	16	15.88059098
GO:1901605	BP	alpha-amino acid metabolic process	6.22E-16	24	15.20625813
GO:0046395	BP	carboxylic acid catabolic process	7.33E-16	26	15.13469837
GO:0016054	BP	organic acid catabolic process	9.10E-16	26	15.04102136
GO:0006631	BP	fatty acid metabolic process	1.87E-15	35	14.72814362
GO:0016053	BP	organic acid biosynthetic process	1.13E-14	28	13.94720534

GO:1902652	BP	secondary alcohol metabolic process	2.57E-14	21	13.59082882
GO:0008203	BP	cholesterol metabolic process	5.19E-14	20	13.28443763
GO:0046394	BP	carboxylic acid biosynthetic process	7.60E-14	27	13.11931607
GO:1901617	BP	organic hydroxy compound biosynthetic process	1.26E-13	24	12.89808104
GO:0016125	BP	sterol metabolic process	1.67E-13	20	12.77777759
GO:0006066	BP	alcohol metabolic process	1.69E-13	29	12.77173355
GO:0046165	BP	alcohol biosynthetic process	3.44E-13	19	12.46315172
GO:1901606	BP	alpha-amino acid catabolic process	6.31E-13	15	12.20023398
GO:0009063	BP	cellular amino acid catabolic process	8.90E-13	16	12.05061252
GO:0006790	BP	sulfur compound metabolic process	1.25E-12	27	11.90423982
GO:0008652	BP	cellular amino acid biosynthetic process	1.54E-10	12	9.81271741
GO:0016829	MF	lyase activity	1.64E-10	19	9.786398762
GO:0016042	BP	lipid catabolic process	3.10E-10	24	9.509212127
GO:0042445	BP	hormone metabolic process	5.57E-10	20	9.254442728
GO:1901607	BP	alpha-amino acid biosynthetic process	6.52E-10	11	9.185839905
GO:0072521	BP	purine-containing compound metabolic process	4.60E-09	27	8.337268623
GO:0009259	BP	ribonucleotide metabolic process	1.57E-08	25	7.804140251
GO:0035634	BP	response to stilbenoid	2.07E-08	7	7.683326213

As presented in Table 1, the functional pathways enriched in the GO annotations were sorted by their p-values to obtain the top 30 pathways with the most significant enrichment. The top five pathways are as follows: steroid metabolic process, cellular amino acid metabolic process, steroid biosynthetic process, sterol biosynthetic process, and small molecule catabolic process. All of these pathways fall under the category of biological processes. The number of genes associated with each of these top five pathways are 35, 30, 25, 17, and 33, respectively.

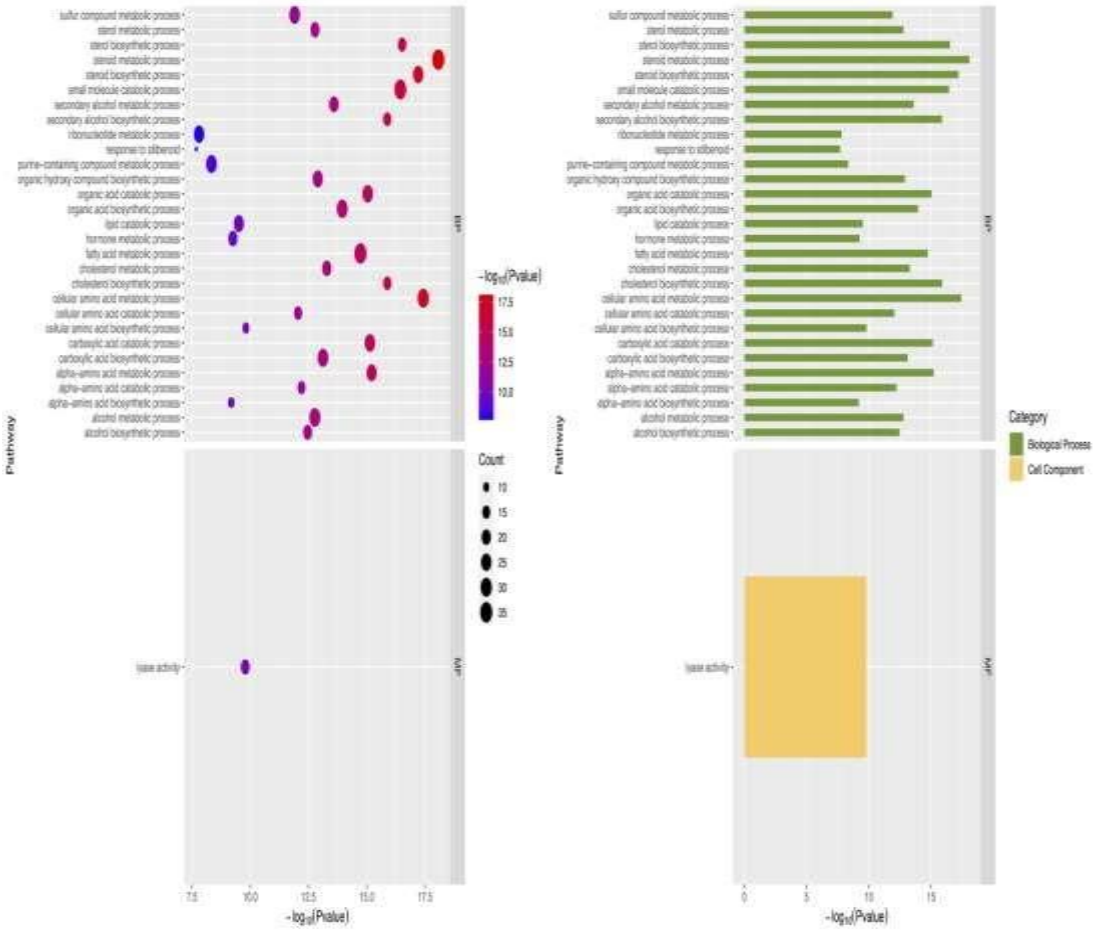

Figure13: GO Bubble chart and histogram

Depicted in Figure 13, the bubble plot and bar chart illustrate the results of the GO enrichment analysis. The bubble plot is configured such that the x-axis represents the statistical measure obtained from the enrichment analysis, while the y-axis denotes the GO terms. Each circle in the plot corresponds to a GO term, with the size of the circle indicating the number of differentially expressed genes within that GO term, and the colour representing the statistical significance, or p-value. In the plot, red indicates a lower p-value, suggesting a more pronounced enrichment of the GO term.

The bar chart, on the other hand, displays only the statistical measures for each GO term, presented as vertical bars. The length of each bar in the chart corresponds to the magnitude of the p-value. A comprehensive analysis of both plots provides a more thorough understanding of the enrichment results. The bubble and bar charts can be used to identify the most significantly enriched GO terms and to ascertain their functional attributes and characteristics[8].
From the analysis of these two graphs, it is evident that the top 30 enriched GO pathways are predominantly categorised under biological processes (BP), accounting for 29 of the pathways, with only one pathway associated with molecular function (MF), and no pathways related to cellular component (CC). This distribution highlights the functional significance of the differentially expressed genes within the context of biological processes.

The Kyoto Encyclopedia of Genes and Genomes (KEGG) is a comprehensive database that encompasses a wide range of biological information, including chemicals, genes, enzymes, metabolic pathways, and

signal transduction pathways. KEGG is primarily utilised for the analysis of metabolic and signal transduction pathways, providing researchers with insights into the metabolic functions and regulatory mechanisms of genes and proteins.

Table2: KEGG enrichment results

	Pathway	pvalue	Count	log10
mmu00100	Steroid biosynthesis - Mus musculus	1.88E-08	8	7.725098757
mmu00830	Retinol metabolism - Mus musculus	7.81E-06	12	5.107349091
mmu00220	Arginine biosynthesis - Mus musculus	8.61E-06	6	5.065074506
mmu00900	Terpenoid backbone biosynthesis - Mus musculus	2.10E-05	6	4.678027629
mmu05171	Coronavirus disease - COVID-19 - Mus musculus	2.60E-05	19	4.585688093
mmu01230	Biosynthesis of amino acids - Mus musculus	3.69E-05	10	4.432428289
mmu00260	Glycine serine and threonine metabolism - Mus musculus	6.88E-05	7	4.162593623
mmu03320	PPAR signaling pathway - Mus musculus	0.000103742	10	3.984046108
mmu00280	Valine leucine and isoleucine degradation - Mus musculus	0.000106983	8	3.970684827
mmu00983	Drug metabolism - other enzymes - Mus musculus	0.000137362	10	3.862134854
mmu00140	Steroid hormone biosynthesis - Mus musculus	0.000150435	10	3.822650579
mmu00071	Fatty acid degradation - Mus musculus	0.0003779	7	3.422623154
mmu00380	Tryptophan metabolism - Mus musculus	0.0003779	7	3.422623154
mmu00350	Tyrosine metabolism - Mus musculus	0.00054991	6	3.259708006
mmu00650	Butanoate metabolism - Mus musculus	0.000593866	5	3.226311667

As detailed in Table 2, the pathways enriched in the KEGG annotations were sorted by their p-values to identify the top 15 pathways with the most significant enrichment. The top five pathways are as follows: Steroid biosynthesis, Retinol metabolism, Arginine biosynthesis, Terpenoid backbone biosynthesis, and Coronavirus disease - COVID-19. The number of genes associated with each of these top five pathways are 8, 12, 6, 6, and 19, respectively.

This ranking of KEGG pathways by enrichment significance offers a focused view on the biological processes and pathways that are most relevant to the differential expression observed in the dataset. The pathways listed suggest areas of metabolic and biological activity that may be particularly affected by the experimental conditions or disease states under investigation.

Table14: KEGG enrichment bubble and histogram

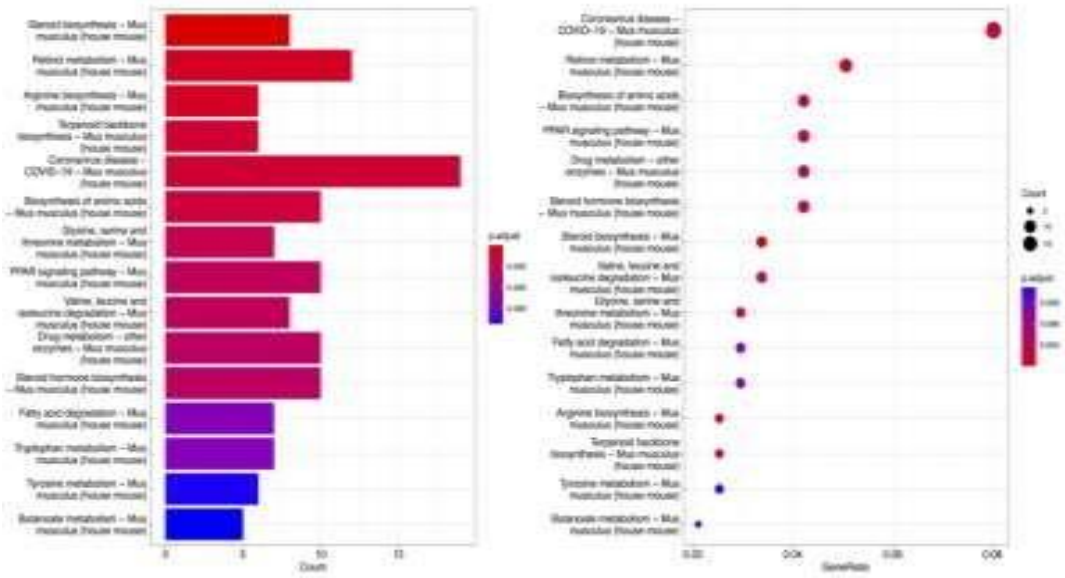

Figure 14 illustrates the bubble plot and bar chart for KEGG pathway enrichment analysis. The bar chart highlights the top 15 pathways that are significantly enriched, with the horizontal axis representing the identified pathways from the enrichment analysis, and the vertical axis indicating the degree of enrichment, commonly depicted by the height of the bars. The variation in colours signifies the level of significance, where red denotes a very low p-value, suggesting a highly significant enrichment of the pathway among the differentially expressed genes.

The bubble plot, on the other hand, visualises the same top 15 KEGG pathways. Here, the horizontal axis corresponds to the enrichment factor, while the vertical axis represents the pathways. Each dot in the plot stands for a pathway, with the size of the dot usually reflecting the number or percentage of differentially expressed genes within that pathway. The colour of the dots indicates the level of significance. Notably, the 'Coronavirus disease - COVID-19' pathway contains the highest number of genes, totaling 19, and the 'Steroid biosynthesis' pathway exhibits the most significant p-value, underscoring its prominence in the dataset.

CONCLUSION

Ginseng flower bud extract has been demonstrated to revert the gene expression associated with fatty liver degeneration, subsequently leading to a significant reduction in lipid droplets stained with Oil Red O and intracellular triglyceride levels in HepG2 cells and rat hepatocytes, thereby exerting an anti-obesity effect. The regulatory genes of GFB are implicated in various aspects, including immune processes, insulin response, and lipid storage. This indicates that ginseng flower bud extract possesses notable anti-obesity properties and may serve as a theoretical reference for subsequent in-depth research.

REFERENCES

[1]Wang, C., Tang, X., Yan, F., Wang, Y., Wang, X., Zhao, D., Liu, L.,
& Qi, B. (2025). Different processing methods affect the chemical composition and in vitro anti-tumor activity of ginseng. Journal of Food Science, 90, e17639. https://doi.org/10.1111/1750-3841.17639

[2]Wei, W., Liu, L., Liu, X., Tao, Y., Gong, J., Wang, Y., & Liu, S. (2022). Black ginseng protects against Western diet-induced nonalcoholic steatohepatitis by modulating the TLR4/NF-κB signaling pathway in mice. Journal of Food Biochemistry, 46, e14432. https://doi.org/10.1111/jfbc.14432

[3]Du, Lian-Yun, Zhang, Hui-E., Zhang, Ye, Han, Yan-Yan, Ye, Ping, Meng, Xiang-Ru, Shen, Yan
-Long, Chen, Chang-Bao, Fan, Mei-Ling, Wang, En-Peng, Comparative Study on Chemical Constituents of Ginseng Flowers with Four Consecutive Cultivation Age, International Journal of Analytical Chemistry, 2023, 1771563, 12 pages, 2023. https://doi.org/10.1155/2023/1771563

[4]Du, Lian-Yun, Zhang, Hui-E., Zhang, Ye, Han, Yan-Yan, Ye, Ping, Meng, Xiang-Ru, Shen, Yan
-Long, Chen, Chang-Bao, Fan, Mei-Ling, Wang, En-Peng, Comparative Study on Chemical Constituents of Ginseng Flowers with Four Consecutive Cultivation Age, International Journal of Analytical Chemistry, 2023, 1771563, 12 pages, 2023. https://doi.org/10.1155/2023/1771563

[5]Zhang, Qiang, Zhang, Li, Liu, Kaili, Shang, Haonan, Ruan, Jun, Yu, Zhonghai, Meng, Sheng xi, Liang, Fang, Wang, Tianzhan, Zhang, Hongyan, Peng, Wenbo, Wang, Yuxin, Chen, Junming , Xiao, Tiegang, Wang, Bing, A Network Pharmacology Study on the Active Components and

Targets of the Radix Ginseng and Radix Bupleuri Herb Pair for Treating Nonalcoholic Fatty Liver Disease, Evidence-Based Complementary and Alternative Medicine, 2022, 1638740, 18 pages, 2022. https://doi.org/10.1155/2022/1638740
[6]Yanming Bai, Shuang Liang, Yanhao Zhou, Bo Zhou, Transcriptomic analysis reveals pharmacological mechanisms mediating efficacy of Yangyinghuoxue Decoction in
CCl4-induced hepatic fibrosis in rats, Frontiers in Pharmacology,
10.3389/fphar.2024.1364023, 15, (2024)
[7]Jin-Jin Dai, Ya-Fei Zhang, Zhen-Hua Zhang, Global trends and hotspots of treatment for nonalcoholic fatty liver disease: A bibliometric and visualization analysis (2010-2023), World Journal of Gastroenterology, 10.3748/wjg.v29.i37.5339, 29, 37, (5339-5360), (2023)
[8]Liping Wu, Shuling Zhang, Qi Zhang, Shaofeng Wei, Guoze Wang, Peng Luo, [Retracted]
The Molecular Mechanism of Hepatic Lipid Metabolism Disorder Caused by NaAsO2 through
Regulating the ERK/PPAR Signaling Pathway, Oxidative Medicine and Cellular Longevity, 10.1155/2022/6405911, 2022, 1, (2022)